IEEE Access
Multidisciplinary | Rapid Review | Open Access Journal

Received April 27, 2019, accepted June 6, 2019, date of publication June 21, 2019, date of current version October 4, 2019.

Digital Object Identifier 10.1109/ACCESS.2019.2924273

Isolation and Identification of Compound Faults in Rotating Machinery via Adaptive Deep Filtering Technique

CHUNLIN ZHANG[1], YULING LIU[2], FANGYI WAN[1], BINQIANG CHEN[3], AND JIE LIU[1,4], (Senior Member, IEEE)

[1]School of Aeronautics, Northwestern Polytechnical University, Xi'an 710072, China
[2]School of Management, Northwestern Polytechnical University, Xi'an 710072, China
[3]School of Aerospace Engineering, Xiamen University, Xiamen 361005, China
[4]Department of Mechanical and Aerospace Engineering, Carleton University, Ottawa, ON K1S5B6, Canada

Corresponding author: Yuling Liu (kaixuanlin123@163.com)

This work was supported in part by the Fundamental Research Funds for the Central Universities under Grant 31020191A009, and in part by the China Postdoctoral Science Foundation under Grant 2018M631196.

ABSTRACT Compound defects commonly occur on rotating machinery under fatigue and heavy loads, and their fault signatures are coupled and easily buried in strong unwanted vibrations and background noise. The isolation and identification of the compound fault signatures are still a challenge especially when the transient impulses induced from the compound defects share common resonant frequency. In this paper, a data-driven, adaptive deep filtering technique which mainly contains filtering and isolating procedures is proposed for compound faults diagnosis. During the filtering procedure, an empirical wavelet transform (EWT) based correlated kurtogram is presented to adaptively obtain the proper spectral segments for filtering the vibration measurements, such that to enhance the signal-to-noise ratio (SNR) of compound faults in the filtered signals. Subsequently, during the isolation procedure, windowed correlated kurtosis (WCK) which outputs pure periodic pulses indicating the occurrence moments of interested fault impulses is presented to isolate each interested fault mode and to determine the defects number. The performance of the proposed technique is tested on simulated signals and validated via analyzing experimental measurements from high-speed locomotive bearings which suffer multiple damages. The results validate that the proposed method outperforms dyadic wavelet transform and spectral kurtogram in isolating and identifying compound faults in rotating machinery.

INDEX TERMS Adaptive deep filtering, compound faults isolation, empirical wavelet transform, fault diagnosis, windowed correlated kurtosis.

I. INTRODUCTION

Bearings and gears are the key parts for supporting and torque transmitting in rotating machinery, and may suffer local damages under fatigue loads and harsh working conditions [1]. Vibrations measured from the machinery housing usually contain the operation information of the bearings and gears, and provide feasible approach for fault diagnosis via signal processing methods [2]–[4].

Based on the fault mechanism, a set of periodic impulses are induced in the vibrations when the local defect collides with contacted rotating components, and different fault characteristic frequencies correspond to different defects locating on different components. To date, much research efforts have been conducted on single fault detection of rotating machinery, and numerous vibration based signal processing methods have been proposed, such as dyadic wavelet transforms [5]–[9], ensemble empirical mode decomposition (EEMD) [10]–[12], spectral kurtosis (SK) [13]–[16], multi-wavelet transform [17]–[19], rational dilation based wavelet transforms [20]–[23], stochastic resonance [24] with nonlinear bistable [25]–[27] or tristable oscillators [28], [29], and intelligent classification methods [30]–[33], etc. Most of these methods are filtering based techniques in which the vibration measurements are divided into several adjacent subbands in the frequency domain and the sensitive subband

The associate editor coordinating the review of this manuscript and approving it for publication was Zhenbao Liu.

possessing the highest SNR of the fault information is then chosen to reveal the fault signature. The effectiveness of these methods has been widely validated via experiment and engineering data analysis, and some of which are found also effective in extracting weak fault signature of rotating machinery in the early defect stage [15].

Beside the widely concerned single defect, multiple faults also commonly occur in rotating machinery under harsh working conditions which are mainly twofold: multiple faults locating in different rotating machinery parts such as rotor damage coupled with bearing or gearbox damages; and multiple faults locating in different components of the same rotating machinery part such as outer-race damage coupled with inner-race or roller damage in the rolling bearings. For multiple faults occurring in different machinery parts, either the fault modes from different machinery parts are different, i.e., harmonic fault feature from rotor damage and impulsive feature from bearing or gear damages, or the compound fault signatures from the bearing and gearbox damages locate in different frequency ranges. Some methods have been proposed for diagnosing this kind of compound faults. Filtering based methods including Morlet wavelet filter [34], multi-wavelets [35], DWT based statistical approach [36], flexible analytical wavelet transform (FAWT) [37], SK [38]–[40], and resonance based decomposition [41] were utilized for detecting compound fault signatures locating in different frequency ranges. Besides, self-adaptive decomposition methods including EMD [42], [43], variational mode decomposition (VMD) [44], and EEMD [45]–[47] methods were also studied and successfully applied on isolating compound faults with different fault modes.

While for the multiple faults which occur in different components of the same rotating machinery part such as defects on different components of the bearing, the fault signatures are essentially several sets of periodic transient impulses. Considering transient impulses are induced in the vibration signals during the collision of the local defects with respect to the contacted components which are essentially similar to the structural impact modal test, the frequency responses of several sets of fault impulses locate at or very close to the natural frequency of the damaged machinery part, i.e., the fault signatures may locate in the same frequency range. Considering this kind of multiple faults are compound in both the time and frequency domain, it is termed 'compound faults' in this study. In such cases, these aforementioned frequency filtering and adaptive decomposition based methods cannot be directly applied for isolation and identification of compound faults, and only a few attempts have been conducted [48], [49]. There remains a critical need for novel technique to isolate and identify the impulsive, compound faults which possess a common resonant frequency.

In this paper, a data driven, adaptive deep filtering technique is proposed for isolating each fault mode from compound fault impulses even when they share the common resonant frequency. The technique mainly contains two steps: empirical wavelet transform (EWT) based filtering and faults isolation. During the filtering step, an empirical wavelet transform (EWT) based correlated kurtogram is presented to adaptively obtain the proper spectral segments for filtering the vibration measurements, such that to enhance the signal-to-noise ratio (SNR) of compound faults in the filtered signals. Subsequently, during the isolation procedure, windowed correlated kurtosis (WCK) is proposed to isolate each interested impulsive fault mode. WCK is inspired by correlated kurtosis (CK). Instead of being an index as the CK to reveal the richness of certain-period fault impulses in tested signals, WCK is an algorithm which outputs periodic pure pulses indicating the occurrence moments of interested fault impulses. Accordingly, each impulsive fault mode is isolated via WCK and the fault signature can be further captured on the envelope spectrum.

The rest of this paper is organized as follows. EWT is briefly introduced in Section II. Section III presents the proposed WCK algorithm and explains the procedures of the adaptive deep filtering technique. The performance of the proposed method is tested on simulated signals in Section IV, and is also compared with existing methods including dyatic wavelet transform and spectral kurtogram via analyzing experiment data tested from a locomotive bearing suffing three outer race defects and two inner race defects in Section V. Finally, conclusions are drawn in Section VI.

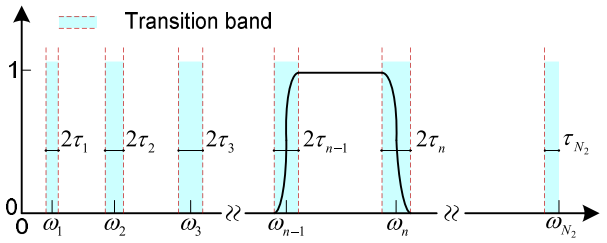

FIGURE 1. Frequency partition manner of the EWT.

II. BRIEF INTRODUCTION OF EMPIRICAL WAVELET TRANSFORM (EWT)

EWT is originally proposed by Gilles [50] for adaptively extracting different modes of the input signals which are assumed to possess compact support in the frequency spectrum. Denoting the frequency response of a time domain signal x as $\widehat{f}(\omega)$ which is normalized in the range $[0, \pi]$, $\widehat{f}(\omega)$ is further divided into N_2 sub-intervals $\Lambda_n = [\omega_{n-1}, \omega_n]$ $(n = 1, 2, \ldots, N_2)$ which meet $\mathrm{U}_{n=1}^{N_2} \Lambda_n = [0, \pi]$. ω_n is the frequency boundary of the Fourier spectrum segment Λ_n and satisfies $\omega_0 = 0$ and $\omega_{N_2} = \pi$, as shown in Figure 1. Around each ω_n a transition phase with width $2\tau_n$ is generated where $\tau_n = \gamma\omega_n$ and $0 < \gamma < 1$. EWT is then defined on each Λ_n in the frequency domain, generating a bank of band-pass filters. Based on Meyer's and Littlewood-Paley wavelets, a wavelet tight frame is proposed in [50], in which the Fourier spectra of the scaling function

and wavelet function are given as:

$$\widehat{\phi}(\omega) = \begin{cases} 1, & \text{if } |\omega| \le \omega_n - \tau_n \\ \cos\left[\frac{\pi}{2}\beta\left(\frac{1}{2\tau_n}(|\omega| - \omega_n + \tau_n)\right)\right], & \\ & \text{if } \omega_n - \tau_n \le |\omega| \le \omega_n + \tau_n \\ 0, & \text{otherwise} \end{cases} \quad (1)$$

$$\widehat{\psi}(\omega) = \begin{cases} 1, & \text{if } \omega_n + \tau_n \le |\omega| \le \omega_{n+1} - \tau_{n+1} \\ \cos\left[\frac{\pi}{2}\beta\left(\frac{1}{2\tau_{n+1}}(|\omega| - \omega_{n+1} + \tau_{n+1})\right)\right], & \\ & \text{if } \omega_{n+1} - \tau_{n+1} \le |\omega| \le \omega_{n+1} + \tau_{n+1} \\ \sin\left[\frac{\pi}{2}\beta\left(\frac{1}{2\tau_n}(|\omega| - \omega_n + \tau_n)\right)\right], & \\ & \text{if } \omega_n - \tau_n \le |\omega| \le \omega_n + \tau_n \\ 0, & \text{otherwise} \end{cases} \quad (2)$$

where $\beta(x)$ determines the shape of the transition band and satisfies $\beta(x) + \beta(1-x) = 1, x \in [0, 1]$ to avoid energy leakage during the transition band. A widely-used function of $\beta(x)$ is proposed by Daubechies [51] and developed by Gilles [50].

$$\beta(x) = x^4\left(35 - 84x + 70x^2 - 20x^3\right) \quad (3)$$

Based on the constructed EWT frame, the vibration measurements are divided into subbands. For an input signal x whose frequency spectrum is denoted as $\widehat{f}(\omega)$, the generated detail and approximation coefficients are calculated via the inner product operation:

$$W_f(n, t) = \langle x, \psi_n(t)\rangle = \text{IFT}\left(\widehat{f}(\omega), \overline{\widehat{\psi}_n(\omega)}\right) \quad (4)$$

$$W_f(0, t) = \langle x, \phi_1(t)\rangle = \text{IFT}\left(\widehat{f}(\omega), \overline{\widehat{\phi}_1(\omega)}\right) \quad (5)$$

where $\psi_n(t)$ and $\phi_1(t)$ are the time-domain functions of the wavelet function $\widehat{\psi}_n(\omega)$ and scaling function $\widehat{\phi}_1(\omega)$, respectively; $\langle\cdot\rangle$ is the inner product operation; and IFT$(\cdot)$ denotes the inverse Fourier transform.

It is clear that the key issue of EWT is the segmentation of the Fourier spectrum. The scale-space segmentation method has been validated to be effective in extracting the primary harmonic components of the input signals [52]. Recalling the input signal x whose frequency spectrum is denoted as $\widehat{f}(\omega)$, the continuous scale-space representation is estimated via the convolution production of $\widehat{f}(\omega)$ and a kernel function $g(\omega; \lambda) = \frac{1}{\sqrt{2\pi\lambda}} \cdot e^{-\omega^2/(2\lambda)}$ where λ is the scale parameter.

$$L(\omega; \lambda) = g(\omega; \lambda) * \widehat{f}(\omega) \quad (6)$$

The local minima of $L(\omega; \lambda)$ is then detected and displayed on the scale-space plane (λ, ω). With increment of the scale parameter λ, these minima produce the "scale-space curves" in the plane (λ, ω). Considering the width of the kernel function $g(\omega; \lambda)$ increases with increment of λ, the number of the minima is thus a decreasing function of the parameter λ. The "scale-space curves" are assumed to be the spectrum boundaries if they last for sufficiently long range of λ. The k-means clustering algorithm is usually adopted to evaluate the threshold of λ for defining the long scale-space curves, after which the boundaries of the Fourier segments are obtained via the projection of these long scale-space curves on the axis ω.

The scale-space segmentation has been validated to be effective in extracting the primary harmonic modes in the vibration signals. However, these isolated harmonic segments could not be directly used to reveal the signature of periodic fault impulses which is a set of sideband frequencies. Accordingly, EWT based correlated kurtogram is developed to merge the possible harmonics and optimize the filtering frequency band.

III. PROPOSED ADAPTIVE DEEP FILTERING METHOD

The adaptive deep filtering technique contains two steps: EWT based correlated kurtogram for adaptive filtering of the raw vibration signals; and WCK for isolation and identification of the compound faults from the filtered signal. In this section, part A presents the algorithm of EWT based correlated kurtogram for filtering the original vibration measurements; WCK is presented in part B, and tested in part C; then the whole procedures of the proposed technique are summarized in part D.

A. EWT BASED CORRELATED KURTOGRAM

Based on the Fourier segments obtained by the scale-space segmentation method, the ensemble EWT subbands are defined to generate possible coalition of these harmonic components, and the correlated kurtogram is further estimated for selecting the optimized filtering subband. The procedure is composed of the following steps:

Step (i) Decomposing the vibration signals using the EWT and reconstructing the filtered signals in each Fourier segment. Assuming that the frequency is divided into N_2 Fourier segments, the filtered signal in each segment is denoted as $\left\{D_k^1 \,|k = 1, 2, \ldots, N_2\right\}$. It is noted D_k^1 are filtered subband signals around different primary harmonics and are orthogonal with each other in the frequency domain.

Step (ii) Constructing the ensemble EWT subbands from the orthogonal subbands using the following formula:

$$D_k^i = \sum_{j=k}^{j=k+i-1} D_j^1, \quad i = 1, 2, \ldots, N_2 + 1 - k \quad (7)$$

where i is the level index; and k is the subband index. Figure 2 schematically show the frequency-level paving manner of the ensemble EWT subbands.

At the level i, D_k^i essentially denotes the combination of i-continuous segments starting from D_k^1 to D_{k+i-1}^1, and $D_1^{N_2}$ is thus the original vibration signal. It is clear that the ensemble EWT subband is a redundant partition of the Fourier spectrum, and the frequency support for D_k^i is estimated to be $\mathrm{U}_{n=k}^{n=k+i-1}\Lambda_n = [\omega_{k-1}, \omega_{k+i-1}]$. In Figure 2, the frequency range for D_k^i is composed of successive subbands which are schematically covered using the same color. Taking the primary harmonics as the basic elements, the ensemble

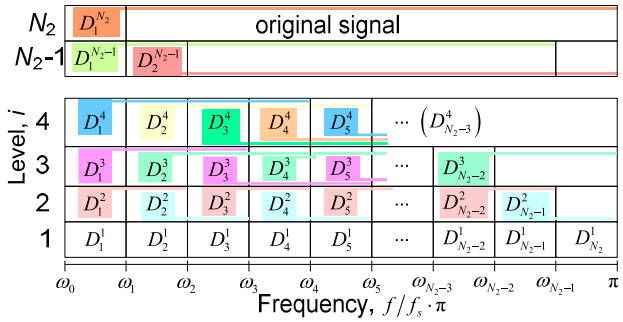

FIGURE 2. Frequency-level paving manner of the ensemble EWT subbands.

EWT subbands provide all potential divisions of the Fourier spectrum.

Step (iii) Calculating the correlated kurtosis of each ensemble EWT subband in Figure 2, i.e., $CK_M\left(D_k^i; T_s\right)$via (8) where T_s is estimated from the interested fault mode. These estimated CK values are further shown on the frequency-level plane (ω, i), which is termed "EWT based correlated kurtogram" exhibiting the CK distribution for the different, redundant frequency subbands.

Step (iv) Optimizing the filtering frequency band and subsequently obtaining the corresponding filtered signals. The CK has been found to usually output large for periodic fault impulses. Considering the ensemble EWT subbands are redundant and the upper lever is essentially the frequency extension of the lower laver, the CK values of the adjacent subbands related to the fault impulses are comparatively high and exhibit "clustering" characteristic. This "clustering" feather could help to increase the robustness of CK index for selecting the proper filtering band. The subband possessing the highest CK value in the clustering zone corresponds to the optimal filtering band, and this is an effective strategy in analyzing engineering data.

B. DEFINITION OF THE WINDOWED CORRELATED KURTOSIS (WCK)

Though the SNR of the fault signature is enhanced in the filtered signal, certain-level noise still exists and the multiple faults are still compound in the filtered signal. WCK is thus proposed for further enhance the SNR and isolate each fault mode from the filtered signal. The WCK is developed from the correlated kurtosis (CK) which was firstly proposed by McDonald *et al.* [39]. For an input signal sequence y_n where $n = 1, 2, 3, \ldots N$, the CK of M-shift for is defined as [40]:

$$CK_M\left(y_n; T_s\right) = \frac{\sum_{n=1}^{N}\left(\prod_{m=0}^{M} y_{n-mT_s}\right)^2}{\left(\sum_{n=1}^{N} y_n^2\right)^{M+1}} \tag{8}$$

in which, M is the order of shift; T_s is the sampling points of the interested period of fault impulses and is estimated via

$$T_s = round\left[f_s \cdot T\right] \tag{9}$$

where f_s is the sampling frequency; T denotes the period of interested fault impulses which is determined by the geometry parameters of the rotating machinery parts and the rotating speed; and *round* represents the rounding operation to obtain the closest integer. It could be found that CK outputs large if periodic impulses with period T exist in the tested signal y_n. Thus, CK has been validated as an effective index to reveal the richness of periodic fault impulses with interested period in the tested signals. However, recalling (8) which takes all the signal points into consideration, CK exhibits the overall characteristic of the input signal and is thus unable to uncover the exact occurrence moments of interested fault impulses in the tested signals.

Inspired by the short-time Fourier transform (STFT) in which the windowing operation enables the capture of the instantaneous time-frequency information during the window interval, the WCK is defined as the CK of windowed signals in which the window width is set as $M \cdot T_s$.

$$WCK_M\left(n, T_s\right) = \frac{\left(\prod_{m=0}^{M} y_{n-mT_s}\right)^2}{\left(\sum_{k=n-MT_s}^{n} y_k^2\right)^{M+1}} \tag{10}$$

From (10), WCK essentially calculates the inner product of signal points with interval T_s during the limited window width, and outputs large when y_n locates at one peak of the interested fault impulses. Accordingly, WCK is supposed to output large indicating the occurrence moments of interested fault impulses, and the fault signature can be captured on its envelope spectrum. Moreover, the difference between WCK and CK is noted here: CK outputs a single value for inputted signals and is usually utilized as an index for filtering subband selection; while WCK outputs a sequence sharing the same length with the inputs and is here an algorithm to isolate interested fault mode from compound-fault signals.

C. PERFORMANCE OF WCK AGAINST THE NOISE

From (10), WCK is a time domain processing method, and its performance against the background noise is tested in this section.

Considering a simulated signal x_1 consisting of a series of periodic impulses x_{11} to approximately simulate the vibration measurements from defected outer race of a rolling bearing, and background Gaussian noise $n(t)$, the expressions are given as

$$x_1(t) = x_{11}(t) + n(t) \tag{11a}$$

$$x_{11}(t) = \sum_{i=1,2,\ldots} e^{-300(t-i/15)} \cdot \cos\left[2\pi \cdot 500 \cdot (t - i/15)\right] \tag{11b}$$

The period of the periodic fault impulses is $T = 1/15$s. Adopting the sampling frequency $f_s = 9000$Hz, an example of the simulated signal is shown in Figure 1(a) in which the SNR is set as -9dB. Take the CK as the index for estimating the shift order, M is evaluated to be 1 since the largest CK is obtained at $M = 1$. Recalling $T_s = f_s \cdot T = 600$,

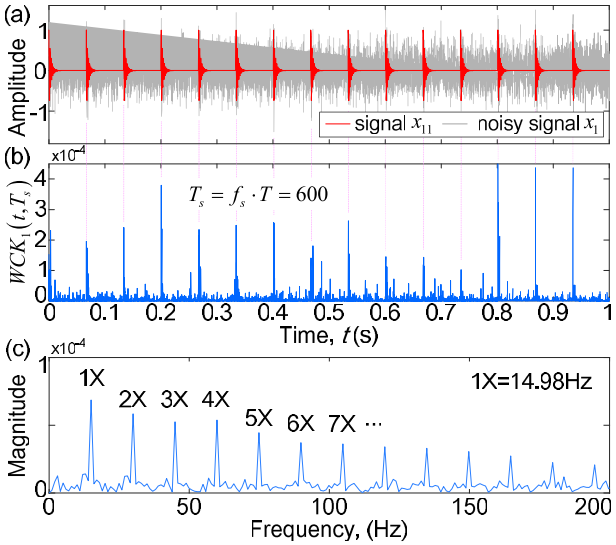

FIGURE 3. Example of WCK algorithm in extracting periodic fault impulses from the noisy signals, in which (a) is simulated signal; (b) is WCK outputs; and (c) envelope spectrum of (b).

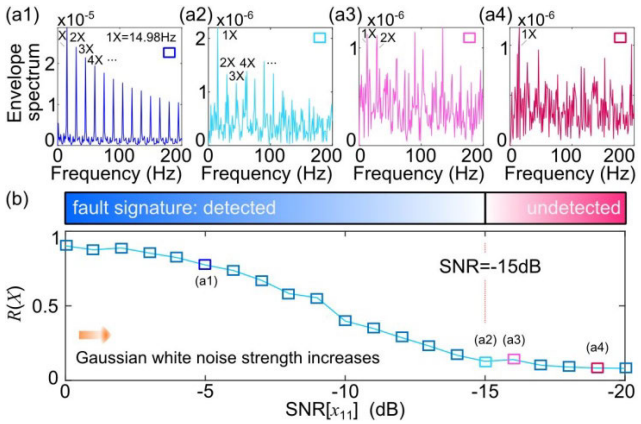

FIGURE 4. Performance of WCK against the noise in which (a) is the envelope spectrum of the output WCK signals with the SNR set at (a1) −5dB; (a2) −15dB; (a3) −16dB; (a4) −19dB; and (b) is the $R(X)$ with respect to different noise strengths.

the WCK of the noisy signal $x_1(t)$ is calculated and displayed in Figure 3(b). It is revealed that WCK outputs periodic pulses indicating the occurrence moments of the interested fault impulses, in which the noise is effectively depressed. Figure 3(c) is the envelope spectrum of the WCK outputs in Figure 3(b), of which the primary components are the fundamental and harmonic components of $1X = 14.98$Hz corresponding to the period of the fault impulses with $T = 1/15$s.

To test the performance of WCK against the background noise, an index $R(X)$ is defined here to quantify the performance of WCK in extracting the impulsive fault signature from noisy signals. Denoting the envelope spectrum of the WCK signals as p_n, $n = 1, 2, \ldots, N_1$ where the data length satisfies $N_1 = N/2$, $R(X)$ is defined as

$$R(X) = \frac{\sum_{i=1,2,\ldots} \left[p_n \big|_{p_n == iX}\right]^2}{\sum_{n=1}^{N_1} p_n^2} \tag{12}$$

in which, X is the repeated frequency of the interested periodic fault impulses. $R(X)$ is essentially the normalized energy of the fundamental fault frequency and its harmonics in the envelope spectrum, and is thus high when the fault signature is successfully captured in the envelope spectrum. Here the performance of WCK is tested on the signal x_{11} polluted by Gaussian white noise with the SNR varying in the range [-20, 0]dB with the interval of 1dB, and $R(X)$ is estimated under each noise strength and shown in Figure 4.

It is revealed that $R(X)$ gradually decreases with increment of the noise strength. Combined with the inserted figures, it is concluded that the performance of the WCK is gradually weakened, and finally fails to isolate interested fault impulses when the SNR is relatively low which is found to be lower than −15dB in the study case.

Accordingly, to apply the WCK on analyzing engineering measurements which contain strong unwanted vibrations and noise, a filtering operation is required as the pre-treatment to enhance the SNR of the compound fault signatures. This is also the reason that EWT based correlated kurtosis is proposed as a prior-processing step in the adaptive deep filtering technique.

D. PROCEDURES OF THE ADAPTIVE DEEP FILTERING TECHNIQUE

The purpose of the adaptive deep filtering technique is to qualitatively isolate and identify each fault mode from the vibration measurements, and to also quantitively determine the defects number. Though the key steps are explained in detail in above, to be more illustrative, the whole procedures of the proposed compound faults isolation and identification method are summarized in the flow char shown in Figure 5.

Overall, the procedures are mainly divided into two steps: first, the EWT based correlated kurtogram is performed on the frequency spectrum of the original vibration signals to adaptively determine the optimal filtering frequency band, such that to enhance the SNR of the compound fault signatures in the frequency filtered signal; second, based on the assumption that different-component faults usually correspond to different fault characteristic frequencies, the WCK algorithm is iteratively conducted on the filtered signals to isolate each interested fault mode with prior predicted fault characteristic frequency. The WCK outputs are pure pulses indicating the occurrence moments of the interested fault mode with the noise further eliminated, based on which the fault signature is captured via identifying the fault characteristic frequency on the Hilbert envelope spectrum of the WCK signal and the defects number is determined via picking up the sets number of the interested periodic pulses.

IV. SIMULATION SIGNAL ANALYSIS

To validate the effectiveness and performance of the proposed method, a numerically simulated signal is generated and

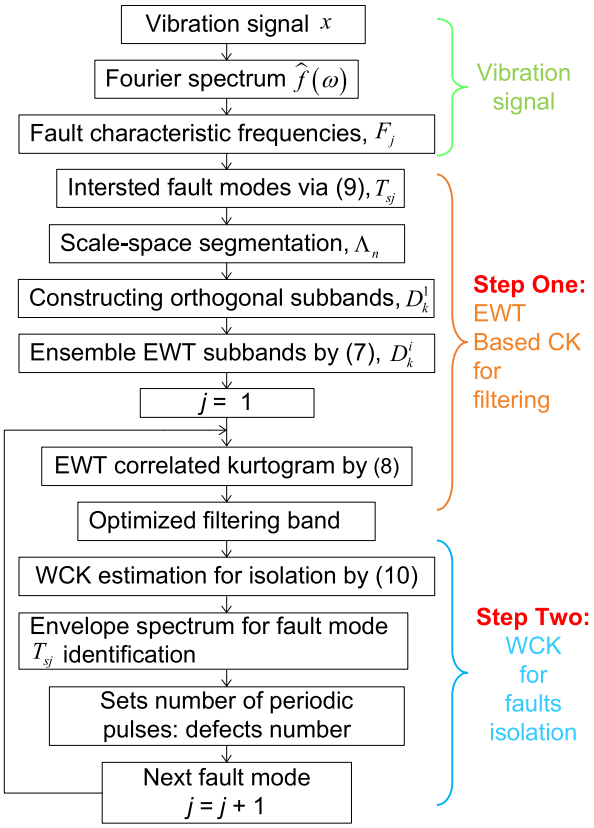

FIGURE 5. Flowchart of the proposed method for compound faults isolation and identification.

TABLE 1. Parameters of the simulated signal x_2.

parameter (unit)	value	parameter (unit)	value
$1/T_1$ (Hz)	18	$1/T_2$ (Hz)	25
f_{n1} (Hz)	300	f_{n2} (Hz)	300
a_1	1.05	a_{21}	1.2
f_r (Hz)	0.6	a_{22}	1.2
ζ	600	ΔT_{21} (s)	0
ΔT_{22} (s)	0.016		

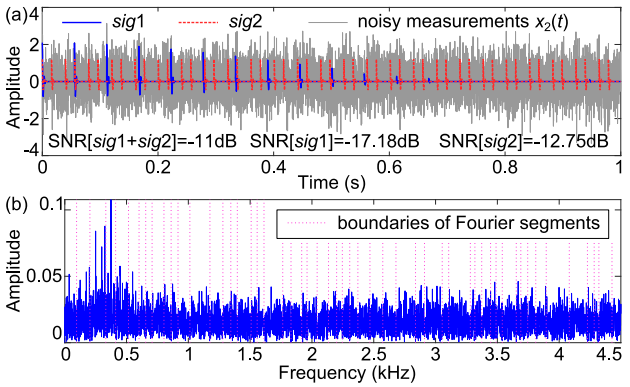

FIGURE 6. The simulated signal and its frequency spectrum, in which (a) is the simulated signal and (b) is the Fourier spectrum segmented via the scale-space method.

analyzed via the proposed method in this section. According to the fault mechanism of the rolling element bearings, the vibration signals induced from damaged bearings are simulated via a series of successive impulses. Considering a roller bearing suffering a local defect on the inner race or roller surface and two local defects on the outer race, a generated signal simulating compound faults is expressed as:

$$x_2 = sig1 + sig2 + n(t) \tag{13a}$$

$$sig1 = \sum_{j=1,2,\ldots} (\cos(2\pi f_r t) + 1) \cdot \left[a_1 e^{-\zeta(t-jT_1)} \cdot \cos(2\pi f_{n1}(t - jT_1))\right] \tag{13b}$$

$$sig2 = \sum_{k=1,2} [\sum_{j=1,2,\ldots} (a_{2k} e^{-\zeta(t-jT_2-\Delta T_{2k})} \cdot \cos(2\pi f_{n2}(t - jT_2 - \Delta T_{2k})))] \tag{13c}$$

in which, $sig1$ is an amplitude-modulated fault signal describing the vibration induced from damaged inner race or roller; $sig2$ is amplitude-constant fault mode which contains two sets of periodic fault impulses with the occurrence time differences denoted as ΔT_{2k}; a_1 is the peak amplitude of periodic impulses $sig1$ whose period is T_1 and oscillating frequency is f_{n1}; f_r is the modulation frequency of the impulse amplitude in $sig1$; a_{2k} is the peak amplitude of $sig2$ the whose period is T_2 and oscillating frequency is f_{n2}; all the fault impulses decay upon the same damping coefficient ζ, and $n(t)$ is the background noise. The selected parameters of the simulated signal x_2 are listed in Table 1.

$n(t)$ is Gaussian white noise. With the SNR of the compound fault signals set as -11dB, Figure 6(a) displays the waveform of the simulated signal in which the sampling frequency is set as 9kHz. It is clear that the tested signal contains two fault modes, i.e., sig1 and sig2, which are totally three sets of periodic fault impulses. Adopting the scale-space segmentation method, the Fourier spectrum is divided into 52 segments corresponding to the primary harmonic components, as shown in Figure 6(b).

Based on the estimated Fourier segments, the tested noisy signal is divided into the Fourier subbands. The ensemble EWT subbands are further constructed based on (11) which represent all potential filtering subbands. Recalling $T_1 = 1/18$s and $T_2 = 1/25$s, the periodic sampling points T_s of the two interested fault modes are estimated to be $T_{s1} = 500$ and $T_{s2} = 360$. It is found the CK value of x_2 reaches highest at $M = 1$, and $M = 1$ is thus selected in estimating the CK values of subband signals. The EWT based correlated kurtogram for the two fault modes are then evaluated and shown in Figure 7.

From Figure 7, the comparatively high CK values in the EWT based correlated kurtogram exhibit "clustering" feature, among which the subband and level indexes corresponding to the maxima, i.e., $(k, i) = (6, 1)$ for the first fault

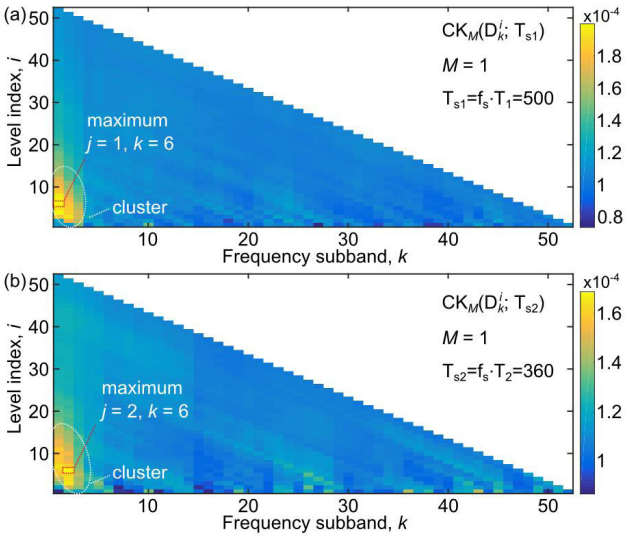

FIGURE 7. EWT based correlated kurtogram for the two fault modes including (a) $CK_1\left(D_k^i; T_{s1}\right)$; and (b) $CK_1\left(D_k^i; T_{s2}\right)$.

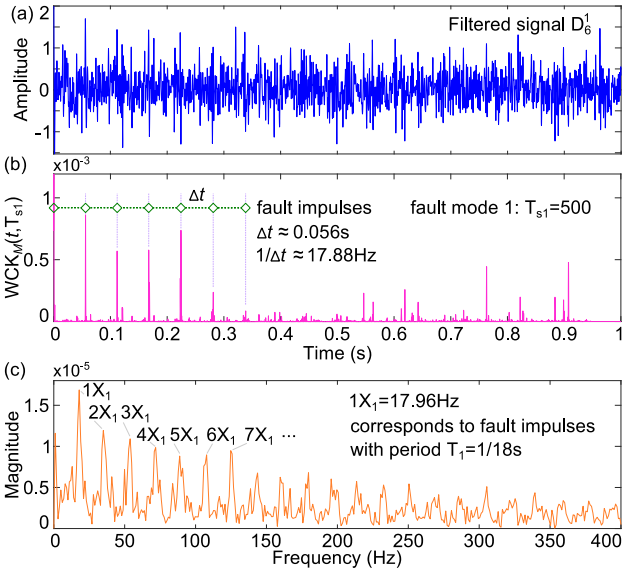

FIGURE 8. Isolation and identification of the first fault mode, in which (a) is the filtered signal; (b) is the WCK signal; and (c) is the envelope spectrum of (b).

mode $T_{s1} = 500$ and $(k, i) = (6, 2)$ for the second fault mode $T_{s2} = 360$, are selected for determining the optimized filtering band. Accordingly, the ensemble EWT subbands D_6^1 and D_6^2 are selected as the filtered signals for detecting the two fault signatures, respectively.

For the first fault mode, the filtered signal D_6^1 is displayed in Figure 8(a). It is noted that the filtered signal contains the compound fault information. To isolate the first fault mode, the WCK algorithm is performed on the filtered signal and the outputs are displayed in Figure 8(b). It reveals that the outputs of the WCK are pure pulses corresponding to the occurrence moments of the primary fault impulses of the sig1.

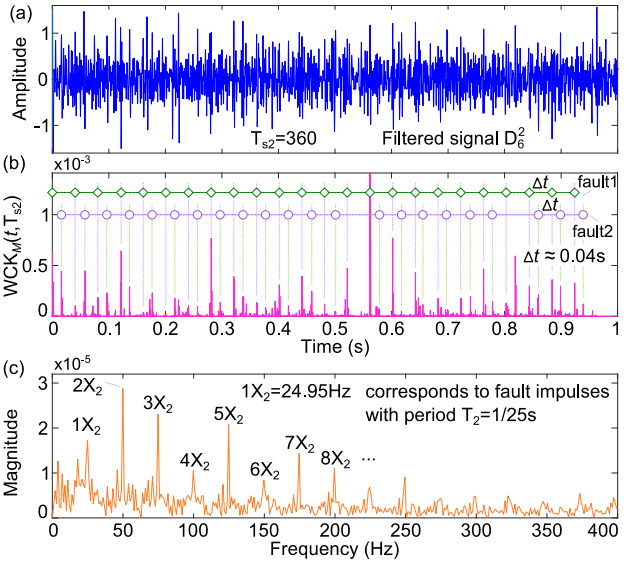

FIGURE 9. Isolation and identification of the second fault mode, in which (a) is the filtered signal; (b) is the WCK signal; and (c) is the envelope spectrum of (b).

The fault signature is also clearly captured from the Hilbert envelope spectrum in Figure 8(c) whose primary components are the fundamental and harmonic components of the fault characteristic frequency $1/T_1 = 18$Hz.

On the other hand, the filtered signal D_6^2 for detecting the second fault mode is displayed in Figure 9(a), and its WCK outputs are given in Figure 9(b). Two sets of periodic pulses are clearly observed in the WCK signals whose period is found to be T_2. The fault signature is also validated from the envelope spectrum of which the primary components are the fundamental and harmonic components of the fault characteristic frequency $1/T_2 = 25$Hz.

From Figures 8 and 9, the two different fault modes, i.e., sig1 and sig2, are successfully isolated, and the number of defects are also effectively estimated via the proposed method. It is thus concluded that for different impulsive fault modes possessing different fault characteristic frequencies (corresponding to compound faults occurred in different components of the rotating machinery), the proposed WCK method is effective in isolating each fault mode; while for compound impulsive faults with the same characteristic frequency (corresponding to compound faults occurred in the same component of the rotating machinery), the WCK outputs are pure pulses in which the unrelated vibration and noise signals are eliminated, and the defects number could be effectively estimated via picking up the sets number of periodic fault impulses. Additionally, the period of the transient fault impulses corresponds to the fault characteristic frequency which is the indicator of the fault signature. It is noted that the fault characteristic frequency highly depends on the geometry parameters, shaft rotating speed and sampling frequency, and is always predicted in prior when analyzing experimental data.

V. EXPERIMENT VALIDATION

A. EXPERIMENTAL TARPED BEARINGS

Experiments are conducted on a double-row tarped roller bearing mounted on the bearing house of the wheelset which is the supporting and braking component in high-speed locomotives, as shown in Figure 10.

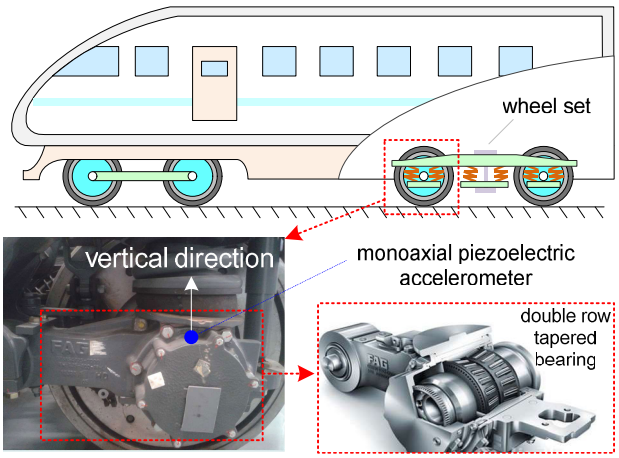

FIGURE 10. Experiments were conducted on a double-row tarped bearing mounted the wheelset of the high-speed locomotive.

The wheelset is fixed on the test rig on which the shaft rotating speed could be exactly controlled such that to simulate the running conditions. A piezoelectric accelerometer typed ZW9609A-18SN7068 was mounted on the bearing house to measure the vibration accelerations in the vertical direction. Multiple local defects are manually prefabricated on the tarped bearing via surface ablation, including three outer race defects and two roller defects. The three outer race defects locate with the central angle of each two was 120°. also, the size of the three defects is 1mm in depth, 1mm, 3mm, and 5mm in width, respectively. The two defected rollers are separated by four healthy rollers (totally 19 rollers in each row), and the size of the defects is 1mm in width and 1mm in depth. It is also noted that the damaged rollers and outer race are in the same row of the double-row tarped bearing.

During the experiments, the locomotive speed is set constantly at 150km/h corresponding to which the rotating frequency of the shaft connected with the inner race is found to be 15.422Hz. Based on the geometry and rotating parameters of the tarped bearing, the fault characteristic frequencies of each component are calculated and listed in Table 2.

TABLE 2. Fault characteristic frequencies of the tested tarped bearing.

component	index	value
shaft	f_i	15.422
outer race	BPFO	124.8837
inner race	BPFI	168.1337
roller	BPF (2BSF)	100.9472
cage	FTF	657.2826

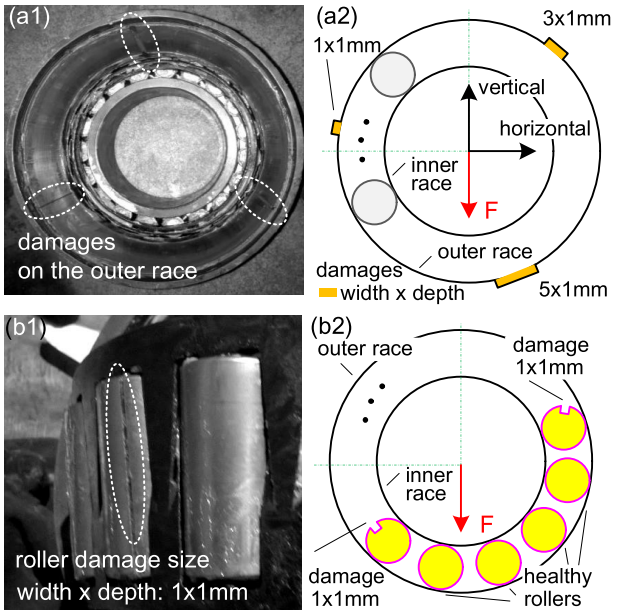

FIGURE 11. Prefabricated multiple defects on the locomotive bearing and their locations and size illustration: (a1) three outer race defects; (a2) locations and size of the outer race defects; (b1) roller defects; and (b2) size of the roller defects.

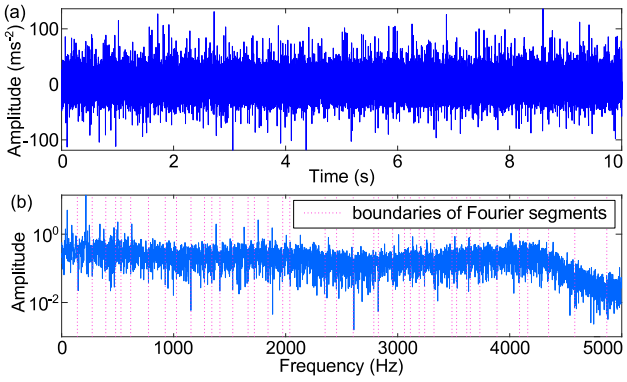

FIGURE 12. (a) Vibration measurements; and (b) Fourier spectrum and its segmentation via the scale-space method.

B. EXPERIMENT DATA ANALYSIS

For healthy bearings, the contacts between the rollers and the inner or outer race are slight in the amplitude and exhibit noise characteristic in the frequency domain. While for the damaged bearings, the collision between the local defect and contacted rotating components are much stronger than that in the healthy case and exhibits periodicity characteristic. The period corresponds to the fault characteristic frequency and is predicted based on the geometry parameters and operating conditions. Considering totally five local defects exist on the tested bearing, it is supposed that five sets of periodic impulses exist in the vibration signals. With the sampling frequency set at 10kHz, the vibration accelerations of the bearing house are measured and shown in Figure 12(a). However, the transient, periodic fault impulses are buried in the strong

background noise and unwanted vibrations, and couldn't be directly observed. Thus, the proposed adaptive deep filtering method is then applied on analyzing the vibration signal to extract the fault modes and determine the defects number. Adopting the scale-space method, the Fourier spectrum in Figure 12(b) is segmented into 42 subbands corresponding to the primary harmonic components.

Based on the determined Fourier boundaries, the EWT is constructed upon which the vibration signal is divided into 42 subband signals denoted as $D_k^1, k = 1, 2, \ldots, 42$. The ensemble EWT subbands D_k^i at each level $i = 1, 2, \ldots, 42$ are then evaluated via (11). Recalling the fault characteristic frequencies (BPFO and BPF) and the sampling frequency, the sampling points of the fault periods are thus $T_{s1} = 80$ for the outer race and $T_{s2} = 99$ for the roller elements. During the calculation of the CK values of the original vibration signal with respect to different values of M, it is found the CK for both the two fault modes reaches the maxima at $M = 1$. The EWT based correlated kurtogram for the two fault modes is then separately estimated via calculating $CK_1\left(D_k^i, T_{s1}\right)$ and $CK_1\left(D_k^i, T_{s2}\right)$ of each ensemble EWT subband signal D_k^i and is shown in Figure 13. It reveals that the comparatively large CK values generate the "clusters" in which the maxima are found at D_3^{24} and D_{13}^5 for detecting the two fault modes, respectively. Accordingly, the filtered signals are D_3^{24} and D_{13}^5, and the corresponding filtering frequency bands are found to be $[273.33, 3061.1]$ Hz and $[1341.1, 1842.2]$ Hz, respectively. The overlapping of the filtering bands indicates that the compound faults are still coexisted in the filtered signals, and the WCK method is further adopted to isolate and identify each fault mode.

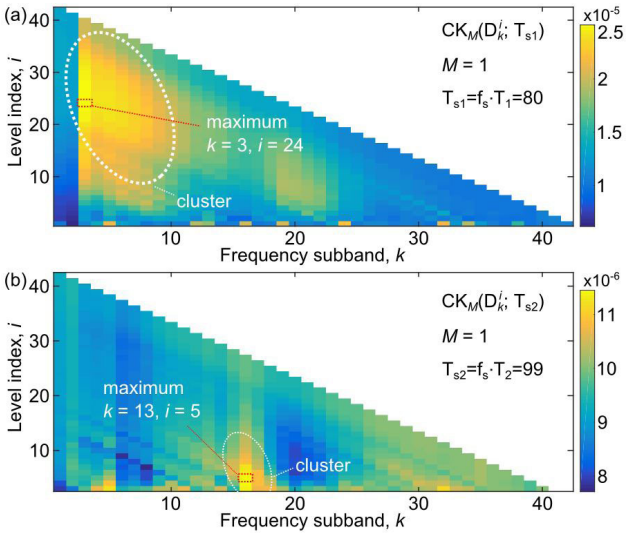

FIGURE 13. EWT based correlated kurtogram for optimizing the filtering band of the two fault modes: (a) outer race defects with $T_{s1} = 80$; and (b) roller defects with $T_{s2} = 99$.

For the outer race defects mode with $T_{s1} = 80$, the filtered signal D_3^{14} is shown in Figure 14(a) in which the periodicity of fault impulses and defects number could not be directly

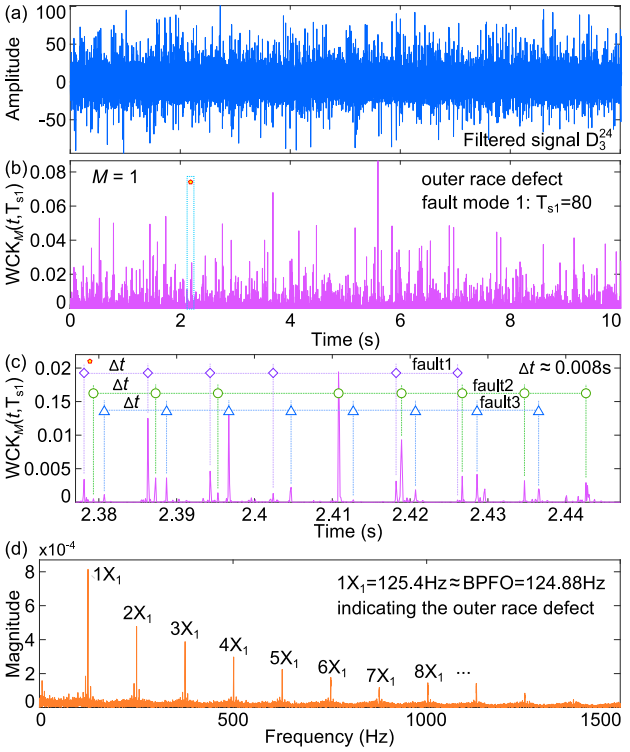

FIGURE 14. Isolation and identification of the outer race defects, in which (a) is the filtered signal; (b) is the WCK outputs; (c) is the zoom-in view of the WCK signal; and (d) is the envelope spectrum of (b).

observed. Then the WCK is performed on the filtered signal and the outputs are displayed in Figure 14(b). Figure 14(c) provides a zoom-in view of the WCK signal. It reveals that the WCK outputs are pure impulses where the noise and unwanted vibrations are effectively eliminated. The WCK outputs also exhibit periodicity and three sets of periodic pulses with the time interval $\Delta t \approx 0.008$s (very close to the reciprocal value of BPFO) are clearly observed, indicating there exists three local defects on the outer race of the locomotive bearing. The fault signature is also exhibited on the envelope spectrum of the WCK signal as shown in Figure 14(d) in which the primary components are the fundamental and harmonic components of the BPFO.

On the other hand, for detecting the roller defects mode with $T_{s2} = 99$, the filtered signal D_{13}^5 is shown in Figure 15(a). the WCK output $WCK_1(t, 99)$ and its zoom-in view are shown in Figs. 15(b) and (c), respectively. The WCK outputs are periodic pulses, and the period is found very close to the BPF and is validated via the envelope spectrum in which the primary components are the fundamental and harmonic components of the BPF. Moreover, there are totally two sets of periodic pulses with the period of $\Delta t \approx 0.01$s which are clearly captured in the WCK outputs, indicating the existence of two local defects on the roller elements.

In this study case, there exists two different fault modes, and totally 5 sets of periodic fault impulses in the vibration measurements. It is concluded that the WCK is effective

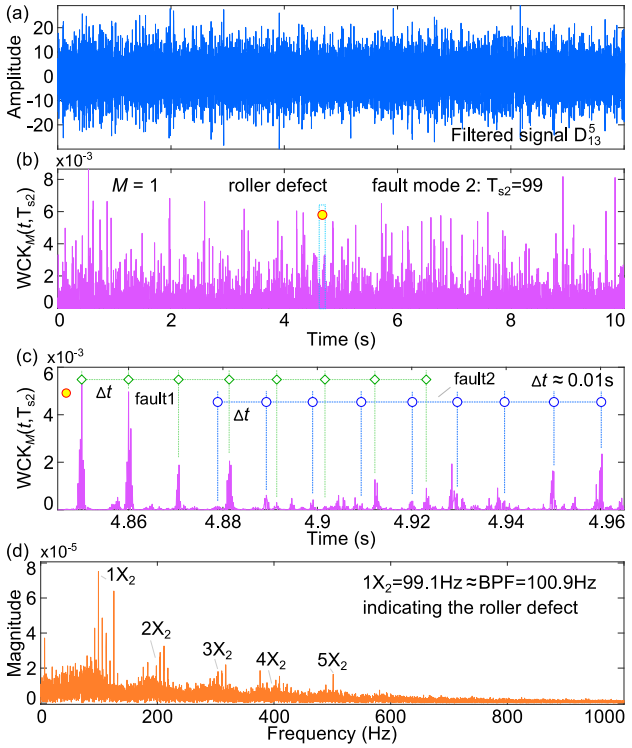

FIGURE 15. Isolation and identification of the roller defects, in which (a) is the filtered signal; (b) is the WCK outputs; (c) is the zoom-in view of the WCK signal; and (d) is the envelope spectrum of (b).

in isolating each fault mode from the filtered signals, and the defects number of the same fault mode is estimated via evaluating the sets number of interested periodic pulses in the WCK signals.

Moreover, to validate the effectiveness of the proposed adaptive deep filtering technique, the experimental data shown in Figure 12(a) are also analyzed via traditional signal processing methods including dual-tree complex wavelet transform (DTCWT) which is a typical dyadic wavelet transform [9] as well as spectral kurtosis [13].

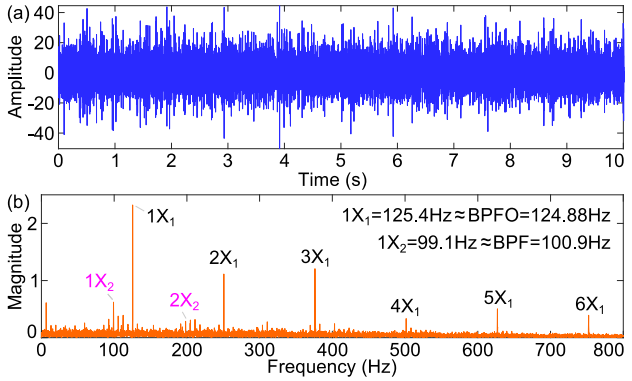

FIGURE 16. Results from the DTCWT including (a) filtered signal by DTCWT; and (b) envelope spectrum of the filtered signal in (a).

Figure 16(a) shows the filtered signal decomposed by the DTCWT, and Figure 16(b) is the envelope spectrum of the filtered signal. Compared with the pure pulses shown in Figure 14(c) and Figure 15(c) which are obtained by the proposed adaptive deep filtering technique, the filtered signals via the DTCWT is still noise contained and exhibit no signature of the defects number. From the envelope spectrum, both the fault characteristic frequencies of the outer race and the roller are observed, meaning the existence of defects on the outer race and the roller. However, compared with the proposed method, the DTCWT possesses weakness in twofold: first, the compound faults are not isolated in the filtered signal, such that the weaker fault signature is easy to be busied in the stronger faults; second, only the fault modes are qualitatively detected, the defects number including three outer race defects and two roller defects could not be successfully identified via the DTCWT.

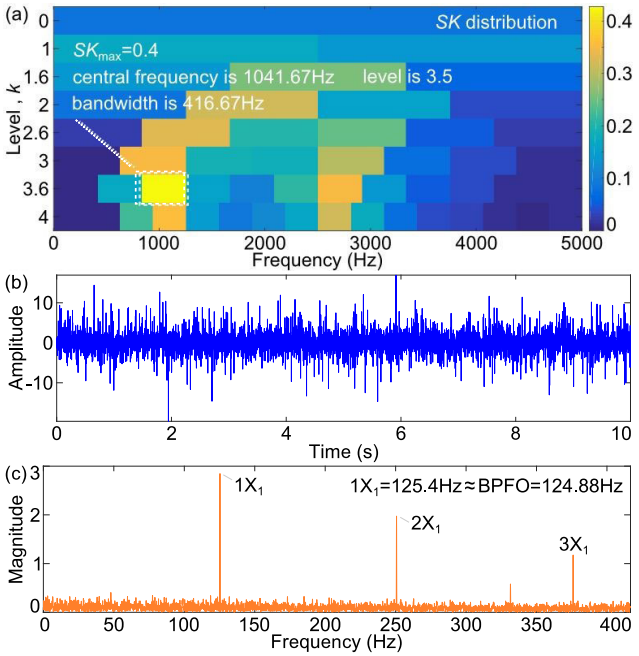

FIGURE 17. Results from the spectral kurtosis method, in which (a) is the SK distribution; (b) is the filtered signal corresponding to the maximal SK value; and (c) is the envelope spectrum of the filtered signal in (b).

Figure 17 shows the analysis result from the spectral kurtosis (SK) method, in which (a) is the SK distribution revealing the kurtosis values of the subband signals decomposed in the frequency-level plane. Based on the kurtosis maximization principle, the maximum is found when the central frequency and the level are 1041.67Hz and 3.5, respectively, and the corresponding filtered signal is displayed in the Figure 17(b). The envelope spectrum of the filtered signal is then estimated and shown in Figure 17(c), of which the primary components are the BPFO and its harmonics. Thus, the SK method only qualitatively detects the outer race defect, while fails to find the roller defect. Compared to the proposed adaptive deep filtering technique, the SK method adopted the kurtosis as the indicator with which the weaker faults are

easily to be ignored in the detection. Additionally, the SK method also fails to estimate the number of the bearing defects.

VI. CONCLUSION

This paper proposed a data driven, adaptive deep filtering technique for isolating and identifying compound fault signatures of the rotating machinery from the noisy vibration signals. The proposed technique mainly consists of filtering and isolation steps. During the route of the proposed technique, the empirical wavelet transform (EWT) based correlated kurtogram is presented for adaptively optimizing the filtering frequency band. The boundaries of the Fourier segments are determined via the scale-space representation with k-means algorithm, upon which the EWT is constructed and the vibration measurements are divided into subband signals corresponding to the primary harmonic components. The ensemble EWT subbands are then constructed which present the potential frequency divisions. The correlated kurtosis of each ensemble EWT subband is calculated, generating the EWT based correlated kurtogram. It is found the CK values of the subbands containing the fault signature are comparatively high and exhibit unique ''cluster'' characteristic on the correlated kurtogram. This unique property helps to enhance the robustness of searching the optimized filtering subband via maximizing the CK index in the ''cluster'' zone. The windowed correlated kurtosis (WCK) algorithm is further adopted for isolating the interested impulsive faults from the filtered signals. Different from CK which is used as an index for revealing the richness of interested fault impulses in the tested signal, the WCK is an algorithm for isolating the interested fault mode. It is found the WCK outputs pure pulses indicating the occurrence moments of interested fault impulses while the noise and unwanted vibrations are eliminated. Via the proposed method, the compound faults are qualitatively isolated and detected, and the defects number of each fault mode is quantitively identified. Moreover, the effectiveness of the proposed method has been tested via simulation signal analysis and validated via experiments on a locomotive tarped bearing suffering three outer race defects and two roller defects. The proposed method has also been compared with existing methods including DTCWT and SK method via analyzing the experiment data. The results show that the proposed method is effective and outperforms DTCWT and SK methods in isolating different fault modes sharing different fault characteristic frequencies. While for compound faults sharing the same fault mode, the defects number could be identified via estimating the sets number of periodic fault impulses in the WCK signals.

ACKNOWLEDGMENT

The authors would like to thank acknowledgment is made to the editors and reviewers for their help in improving the quality of this manuscript.

REFERENCES

[1] Y. Li, X. Wang, Z. Liu, X. Liang, and S. Si, ''The entropy algorithm and its variants in the fault diagnosis of rotating machinery: A review,'' *IEEE Access*, vol. 6, pp. 66723–66741, 2018.
[2] W. He, B. Chen, N. Zeng, and Y. Zi, ''Sparsity-based signal extraction using dual Q-factors for gearbox fault detection,'' *ISA Trans.*, vol. 79, pp. 147–160, Aug. 2018.
[3] H. Jiang, J. Chen, and G. Dong, ''Hidden Markov model and nuisance attribute projection based bearing performance degradation assessment,'' *Mech. Syst. Signal Process.*, vols. 72–73, pp. 184–205, May 2016.
[4] L. Ciabattoni, F. Ferracuti, A. Freddi, and A. Monteriu, ''Statistical spectral analysis for fault diagnosis of rotating machines,'' *IEEE Trans. Ind. Electron.*, vol. 65, no. 5, pp. 4301–4310, May 2017.
[5] N. Bessous, S. E. Zouzou, W. Bentrah, S. Sbaa, and M. Sahraoui, ''Diagnosis of bearing defects in induction motors using discrete wavelet transform,'' *Int. J. Syst. Assurance Eng. Manage.*, vol. 9, pp. 335–343, Apr. 2018.
[6] W. Huang, F. Kong, and X. Zhao, ''Spur bevel gearbox fault diagnosis using wavelet packet transform and rough set theory,'' *J. Intell. Manuf.*, vol. 29, no. 6, pp. 1257–1271, Aug. 2018.
[7] B. Hu and B. Li, ''A new multiscale noise tuning stochastic resonance for enhanced fault diagnosis in wind turbine drivetrains,'' *Meas. Sci. Technol.*, vol. 27, no. 2, Jan. 2016, Art. no. 025017.
[8] W. Sun, B. Yao, N. Zeng, B. Chen, Y. He, X. Cao, and W. He, ''An intelligent gear fault diagnosis methodology using a complex wavelet enhanced convolutional neural network,'' *Materials*, vol. 10, no. 7, p. 790, Jul. 2017.
[9] R. Yan, R. X. Gao, and X. Chen, ''Wavelets for fault diagnosis of rotary machines: A review with applications,'' *Signal Process.*, vol. 96, pp. 1–15, Mar. 2014.
[10] G. Georgoulas, T. Loutas, C. D. Stylios, and V. Kostopoulos, ''Bearing fault detection based on hybrid ensemble detector and empirical mode decomposition,'' *Mech. Syst. Signal Process.*, vol. 41, pp. 510–525, Dec. 2013.
[11] Y. Lei, J. Lin, Z. He, and M. J. Zuo, ''A review on empirical mode decomposition in fault diagnosis of rotating machinery,'' *Mech. Syst. Signal Process.*, vol. 35, nos. 1–2, pp. 108–126, Feb. 2013.
[12] X. Zhang, Z. Liu, Q. Miao, and L. Wang, ''An optimized time varying filtering based empirical mode decomposition method with grey wolf optimizer for machinery fault diagnosis,'' *J. Sound Vib.*, vol. 418, pp. 55–78, Mar. 2018.
[13] J. Antoni and R. Randall, ''The spectral kurtosis: Application to the vibratory surveillance and diagnostics of rotating machines,'' *Mech. Syst. Signal Process.*, vol. 20, no. 2, pp. 308–331, 2006.
[14] B. Chen, Z. Zhang, Y. Zi, Z. He, and C. Sun, ''Detecting of transient vibration signatures using an improved fast spatial–spectral ensemble kurtosis kurtogram and its applications to mechanical signature analysis of short duration data from rotating machinery,'' *Mech. Syst. Signal Process.*, vol. 40, no. 1, pp. 1–37, Oct. 2013.
[15] X. Chen, F. Feng, and B. Zhang, ''Weak fault feature extraction of rolling bearings based on an improved Kurtogram,'' *Sensors*, vol. 16, no. 9, p. 1482, 2016.
[16] H. Wang, J. Chen, and G. Dong, ''Fault diagnosis of rolling bearing's early weak fault based on minimum entropy de-convolution and fast Kurtogram algorithm,'' *Proc. Inst. Mech. Eng., C, J. Mech. Eng. Sci.*, vol. 229, no. 16, pp. 2890–2907, Nov. 2015.
[17] J. Yuan, Y. Wang, Y. Peng, and C. Wei, ''Weak fault detection and health degradation monitoring using customized standard multiwavelets,'' *Mech. Syst. Signal Process.*, vol. 94, pp. 384–399, Sep. 2017.
[18] N. Lu, G. Zhang, Z. Xiao, and O. P. Malik, ''Feature extraction based on adaptive multiwavelets and LTSA for rotating machinery fault diagnosis,'' *Shock Vib.*, vol. 2019, Jan. 2019, Art. no. 1201084.
[19] J. Chen, Z. Li, J. Pan, G. Chen, Y. Zi, J. Yuan, B. Chen, and Z. He, ''Wavelet transform based on inner product in fault diagnosis of rotating machinery: A review,'' *Mech. Syst. Signal Process.*, vols. 70–71, pp. 1–35, Mar. 2016.
[20] C. Zhang, B. Li, B. Chen, H. Cao, Y. Zi, and Z. He, ''Periodic impulsive fault feature extraction of rotating machinery using dual-tree rational dilation complex wavelet transform,'' *J. Manuf. Sci. Eng.*, vol. 136, no. 5, Aug. 2014, Art. no. 051011.
[21] M. Sharma, R. B. Pachori, and U. R. Acharya, ''A new approach to characterize epileptic seizures using analytic time-frequency flexible wavelet transform and fractal dimension,'' *Pattern Recognit. Lett.*, vol. 94, pp. 172–179, Jul. 2017.

[22] J. Singh, A. K. Darpe, and S. P. Singh, "Rolling element bearing fault diagnosis based on over-complete rational dilation wavelet transform and auto-correlation of analytic energy operator," *Mech. Syst. Signal Process.*, vol. 100, pp. 662–693, Feb. 2018.

[23] C. L. Zhang, B. Li, B. Q. Chen, H. R. Cao, Y. Y. Zi, and Z. J. He, "Weak fault signature extraction of rotating machinery using flexible analytic wavelet transform," *Mech. Syst. Signal Process.*, vols. 64–65, pp. 162–187, Dec. 2015.

[24] Y. Qin, Y. Tao, Y. He, and B. Tang, "Adaptive bistable stochastic resonance and its application in mechanical fault feature extraction," *J. Sound Vib.*, vol. 333, no. 26, pp. 7386–7400, Dec. 2014.

[25] C. Zhang, R. L. Harne, B. Li, and K. W. Wang, "Statistical quantification of dc power generated by bistable piezoelectric energy harvesters when driven by random excitations," *J. Sound Vib.*, vol. 442, pp. 770–786, Mar. 2019.

[26] Y. Liu, P. Guo, and C. Zhang, "Transient dynamics and electric power estimation of bistable energy harvesters under impulsive excitations," *IEEE Access*, vol. 7, pp. 36233–36245, 2019.

[27] H. Fang, S. Li, H. Ji, and K. W. Wang, "Dynamics of a bistable Miura-origami structure," *Phys. Rev. E, Stat. Phys. Plasmas Fluids Relat. Interdiscip. Top.*, vol. 95, no. 5, May 2017, Art. no. 052211.

[28] S. Zhou and L. Zuo, "Nonlinear dynamic analysis of asymmetric tristable energy harvesters for enhanced energy harvesting," *Commun. Nonlinear Sci. Numer. Simul.*, vol. 61, pp. 271–284, Aug. 2018.

[29] K. Yang, Z. Zhang, Y. Zhang, and H. Huang, "High-resolution monitoring of aerospace structure using the bifurcation of a bistable nonlinear circuit with tunable potential-well depth," *Aerosp. Sci. Technol.*, vol. 87, pp. 98–109, Apr. 2019.

[30] B. Cai, L. Huang, and M. Xie, "Bayesian networks in fault diagnosis," *IEEE Trans. Ind. Informat.*, vol. 13, no. 5, pp. 2227–2240, Oct. 2017.

[31] W. Chine, A. Mellit, V. Lughi, A. Malek, G. Sulligoi, and A. M. Pavan, "A novel fault diagnosis technique for photovoltaic systems based on artificial neural networks," *Renew. Energy*, vol. 90, pp. 501–512, May 2016.

[32] F. Jia, Y. G. Lei, J. Lin, X. Zhou, and N. Lu, "Deep neural networks: A promising tool for fault characteristic mining and intelligent diagnosis of rotating machinery with massive data," *Mech. Syst. Signal Process.*, vols. 72–73, pp. 303–315, May 2016.

[33] X. Liang, M. J. Zuo, and L. Liu, "A windowing and mapping strategy for gear tooth fault detection of a planetary gearbox," *Mech. Syst. Signal Process.*, vol. 80, pp. 445–459, Dec. 2016.

[34] X. Gu, S. Yang, Y. Liu, F. Deng, and B. Ren, "Compound faults detection of the rolling element bearing based on the optimal complex Morlet wavelet filter," *Proc. Inst. Mech. Eng., C, J. Mech. Eng. Sci.*, vol. 232, no. 10, pp. 1786–1801, May 2018.

[35] J. Chen, Y. Zi, Z. He, and Y. Jing, "Compound faults detection of rotating machinery using improved adaptive redundant lifting multiwavelet," *Mech. Syst. Signal Process.*, vol. 38, no. 1, pp. 36–54, 2013.

[36] W. Fan, Q. Zhou, J. Li, and Z. Zhu, "A wavelet-based statistical approach for monitoring and diagnosis of compound faults with application to rolling bearings," *IEEE Trans. Autom. Sci. Eng.*, vol. 15, no. 4, pp. 1563–1572, Oct. 2018.

[37] C. Zhang, Y. Liu, F. Wan, B. Chen, J. Liu, and B. Hu, "Multi-faults diagnosis of rolling bearings via adaptive customization of flexible analytical wavelet bases," *Chin. J. Aeronaut.*, to be published. doi: 10.1016/j.cja.2019.03.014.

[38] D. He, X. Wang, S. Li, J. Lin, and M. Zhao, "Identification of multiple faults in rotating machinery based on minimum entropy deconvolution combined with spectral kurtosis," *Mech. Syst. Signal Process.*, vol. 81, pp. 235–249, Dec. 2016.

[39] G. L. McDonald, Q. Zhao, and M. J. Zuo, "Maximum correlated Kurtosis deconvolution and application on gear tooth chip fault detection," *Mech. Syst. Signal Process.*, vol. 33, pp. 237–255, Nov. 2012.

[40] Y. Miao, M. Zhao, J. Lin, and Y. Lei, "Application of an improved maximum correlated Kurtosis deconvolution method for fault diagnosis of rolling element bearings," *Mech. Syst. Signal Process.*, vol. 92, pp. 173–195, Aug. 2017.

[41] D. Zhang, D. Yu, and W. Zhang, "Energy operator demodulating of optimal resonance components for the compound faults diagnosis of gearboxes," *Meas. Sci. Technol.*, vol. 26, no. 11, Sep. 2015, Art. no. 115003.

[42] L. Ming, L. Fucai, J. Beibei, B. Huiyu, L. Hongguang, and M. Guang, "Multi-fault diagnosis of rotor system based on differential-based empirical mode decomposition," *J. Vib. Control*, vol. 21, no. 9, pp. 1821–1837, Jul. 2015.

[43] X. Zhang and J. Zhou, "Multi-fault diagnosis for rolling element bearings based on ensemble empirical mode decomposition and optimized support vector machines," *Mech. Syst. Signal Process.*, vol. 41, nos. 1–2, pp. 127–140, Dec. 2013.

[44] Z. Zhang, X. Zhang, P. Zhang, F. Wu, and X. Li, "Compound fault extraction method via self-adaptively determining the number of decomposition layers of the variational mode decomposition," *Rev. Sci. Instrum.*, vol. 89, no. 8, Aug. 2018, Art. no. 085110.

[45] H. Jiang, C. Li, and H. Li, "An improved EEMD with multiwavelet packet for rotating machinery multi-fault diagnosis," *Mech. Syst. Signal Process.*, vol. 36, no. 2, pp. 225–239, 2013.

[46] H. Li, M. Li, C. Li, F. Li, and G. Meng, "Multi-faults decoupling on turbo-expander using differential-based ensemble empirical mode decomposition," *Mech. Syst. Signal Process.*, vol. 93, pp. 267–280, Sep. 2017.

[47] H. Wang, R. Li, G. Tang, H. Yuan, Q. Zhao, and X. Cao, "A compound fault diagnosis for rolling bearings method based on blind source separation and ensemble empirical mode decomposition," *PLoS One*, vol. 9, no. 10, Oct. 2014, Art. no. e109166.

[48] W. He, Y. Ding, Y. Zi, and I. W. Selesnick, "Repetitive transients extraction algorithm for detecting bearing faults," *Mech. Syst. Signal Process.*, vol. 84, pp. 227–244, Feb. 2017.

[49] H. Wang, "Fault diagnosis of rolling element bearing compound faults based on sparse no-negative matrix factorization-support vector data description," *J. Vib. Control*, vol. 24, no. 2, pp. 272–282, Jan. 2018.

[50] J. Gilles, "Empirical wavelet transform," *IEEE Trans. Signal Process.*, vol. 61, no. 16, pp. 3999–4010, Aug. 2013.

[51] I. Daubechies, *Ten Lectures on Wavelets*. Philadelphia, PA, USA: SIAM, 1992.

[52] J. Gilles and K. Heal, "A parameterless scale-space approach to find meaningful modes in histograms—Application to image and spectrum segmentation," *Int. J. Wavelets, Multiresolution Inf. Process.*, vol. 12, no. 6, Nov. 2014, Art. no. 1450044.

CHUNLIN ZHANG received the B.S. and Ph.D. degrees in mechanical engineering from Xi'an Jiaotong University, Xi'an, China, in 2011 and 2017, respectively.

He then joined the School of Aeronautics, Northwestern Polytechnical University, Xi'an, where he is currently an Assistant Professor. From 2014 to 2016, he was a Visiting Scholar with the University of Michigan, Ann Arbor, MI, USA. His main research interests include structural vibrations, dynamics and fault diagnosis, and nonlinear vibration energy harvesting.

YULING LIU received the B.S. degree in management science and technology from Sichuan University, China, in 2010. She is currently pursuing the Ph.D. degree in management science and technology with Northwestern Polytechnical University, China.

Her research interests include nonlinear dynamics, operation reliability assessment, and the maintenance strategy optimization of mechanical structures and equipments.

FANGYI WAN received the B.S. degree in water resources and hydroelectric engineering and the M.S. degree in printing and packaging engineering from the Xi'an University of Technology, Xi'an, China, in 1994 and 1996, respectively, and the Ph.D. degree in mechanics engineering from Xi'an Jiaotong University, Xi'an, China, in 2003.

He then joined the School of Aeronautics, Northwestern Polytechnical University, Xi'an, as a Faculty Member, where he is currently an Associate Professor. He was a Visiting Scholar with the Virginia Polytechnic Institute and State University, VA, USA, from 2005 to 2006, and the University of Liège, Liège, Belgium, from 2013 to 2014. His main research interests include vibration analysis and control, design, modeling, test, and health management of aircraft structures.

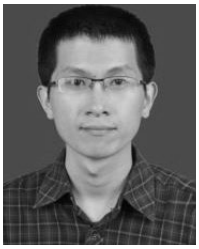

BINQIANG CHEN was born in Fuqing, Fujian, China, in 1986. He received the bachelor's degree in mechanical engineering from the School of Manufacturing Science and Technology, Sichuan University, in 2008, and the Ph.D. degree in mechanical engineering from the School of Mechanical Engineering, Xi'an Jiaotong University, in 2013.

His main research interests include intelligent equipment and smart manufacturing, structural health monitoring of equipment, and applied harmonic analysis.

JIE LIU received the B.Eng. degree in electronics and precision engineering from Tianjin University, Tianjin, China, in 1998, the M.Sc. degree in control engineering from Lakehead University, Thunder Bay, ON, Canada, in 2005, and the Ph.D. degree in mechanical engineering from the University of Waterloo, Waterloo, ON, Canada, in 2008.

He is currently an Associate Professor with the Department of Mechanical and Aerospace Engineering, Carleton University, Ottawa, Canada. He is also a Part-Time Researcher at the School of Aeronautics, Northwestern Polytechnical University, Xi'an, China. His research interests include dynamics, signal processing, vibration analysis and control, linear/nonlinear system control, machine condition monitoring, instrumentation and measurement, mechatronic systems, and artificial intelligence.